Kinetic Analysis of Reactions of *p*-Anisidine and *N*-Methyl-*p*-anisidine Cation Radicals in Acetonitrile Using an Electron-Transfer Stopped-Flow Method

Masashi Goto and Koji Otsuka

Department of Material Chemistry, Graduate School of Engineering, Kyoto University, Sakyo-ku, Kyoto 606-8501, Japan

Xi Chen and Ying Tao

The Key Laboratory of Analytical Sciences of Ministry of Education and Department of Chemistry, Xiamen University, Xiamen 361005, China

Munetaka Oyama*

Division of Research Initiatives, International Innovation Center, Kyoto University, Sakyo-ku, Kyoto 606-8501, Japan

Received: June 5, 2003; In Final Form: February 3, 2004

The chemical follow-up reactions after one-electron oxidation of *p*-anisidine (PA), *N*-methyl-*p*-anisidine (MPA), and *N*-benzyl-*p*-anisidine (BPA) in acetonitrile (AN) were analyzed with a stopped-flow method utilizing the electron-transfer reaction with the tris(*p*-bromophenyl)amine (TBPA) cation radical. The reactions of these *p*-anisidine derivative cation radicals in AN were found to be faster than that of *N*,*N*-dimethyl-*p*-anisidine (DMPA) cation radical, which proceeds via the acid−base interaction between $DMPA^{\bullet+}$ and DMPA. In addition, while the rate law of the decay reaction of $DMPA^{\bullet+}$ was expressed as $-d[DMPA^{\bullet+}]/dt = k[DMPA^{\bullet+}][DMPA]$, that of $PA^{\bullet+}$ has been determined to be $-d[PA^{\bullet+}]/dt = k[PA^{\bullet+}]^2[PA]$ when $PA^{\bullet+}$ was generated in the presence of PA. On the other hand, in the case that $PA^{\bullet+}$ was quantitatively formed without PA via equimolar mixing with $TBPA^{\bullet+}$, the rate was determined to be $-d[PA^{\bullet+}]/dt = k[PA^{\bullet+}]^2$. Also, for the reactions of $MPA^{\bullet+}$ and $BPA^{\bullet+}$, the rate laws were identical to those of $PA^{\bullet+}$. From these results, the reaction mechanisms and the effects of the methyl groups on the reaction kinetics of the *p*-anisidine derivative cation radicals in AN were discussed.

Introduction

The development of fast-scan cyclic voltammetry with ultramicroelectrodes permitted detailed investigations on the electrochemical oxidation processes of aromatic amine cation radicals in aprotic solvents. Owing to this advance, the complex reaction mechanisms of short-lived aromatic amine cation radicals have become apparent.[1−4] The dimerization reactions of diphenylamine and *N*,*N*-dimethylaniline in acetonitrile were studied using this technique, and consequently, the cation radical−cation radical coupling mechanism has been proved.[1,2] Farsang and Amatore investigated the reaction mechanisms of para-substituted anilines in dimethylformamide (DMF), and the complex mechanistic aspects of the cation radicals involving the neutral molecules to form the C−N bonding have been reported.[3,4]

Recently, as an alternative method to observe the reaction process of short-lived aromatic cation radicals, we are proposing an electron-transfer stopped-flow (ETSF) method.[5−8] The reactions of diphenylamine and methyldiphenylamine cation radicals could be successfully analyzed using this ETSF method.[5] Utilizing this technique, we analyzed the reactions of the cation radicals of *N*,*N*-dimethyl-*p*-toluidine[7] and *N*,*N*-dimethyl-*p*-anisidine,[8] and the acid−base interaction between the cation radical and the neutral molecule has been clarified. In these cases, the reaction products were the dimer compounds formed via the C−C bonding of the C atoms of the methyl groups, while the reaction product of *p*-anisidine is known to be formed via the C−N bonding accompanying the elimination of the methoxy group at the para position.[3] The *p*-anisidine cation radical is more reactive, or short-lived, than the *N*,*N*-dimethyl-*p*-anisidine cation radical because two methyl groups on the N atom exhibit a blocking effect to prevent the direct C−N bonding, or other reactions. However, to our knowledge, there are no systematic comparisons or investigations on the effects of the *N*-methyl groups on the reaction kinetics, in particular, on how the reactivity of aniline derivative cation radicals changes kinetically due to the substitution of $-CH_3$ to $-H$.

In the present paper, we thus analyzed the decay reactions of *N*-methyl-*p*-anisidine (MPA) and *p*-anisidine (PA) cation radicals in acetonitrile (AN) using the ETSF method. By comparing the present results with previous ones for *N*,*N*-dimethyl-*p*-anisidine (DMPA) cation radical[8] and observing also the reaction of *N*-benzyl-*p*-anisidine (BPA), we discuss how the reactivity of the cation radicals, or the follow-up chemical reactions, changes in the absence of the *N*-methyl group.

* Corresponding author. Telephone: +81-75-753-9152. Fax: +81-75-753-9145. E-mail: oyama@iic.kyoto-u.ac.jp.

10.1021/jp035579c CCC: $27.50
Published on Web 04/14/2004

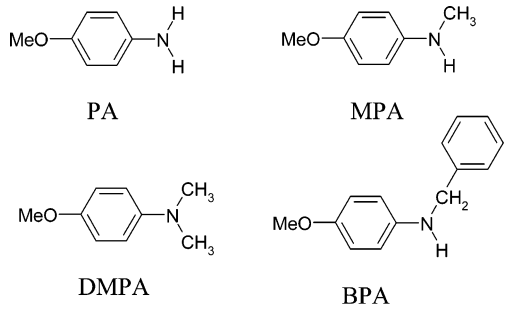

In addition, for the case of $PA^{\bullet+}$, some kinetic conclusions in homogeneous AN solution are presented on the basis of the observed results using the ETSF method, though these are different from those of a previous report.[3] While direct comparison was difficult between the electrochemical reactions in DMF[3] and the homogeneous reactions in AN, the results of the present ETSF observation would be an interesting example to show the complexity of the reactions involving $PA^{\bullet+}$ in AN.

Experimental Section

The details of the ETSF method were described previously.[5−8] Because the oxidation potentials of PA and MPA are very negative compared to that of the tris(*p*-bromophenyl)amine cation radical ($TBPA^{\bullet+}$) as shown later, we mixed AN solutions of PA (or MPA) and $TBPA^{\bullet+}$ to promote the electron transfer for the quantitative generation of short-lived $PA^{\bullet+}$ (or $MPA^{\bullet+}$). After mixing the solutions, dynamic transformation of visible absorption spectra is observable in the optical cell with the minimum time interval of 1.0 ms. The obtained decay curve at a wavelength was composed of 512 points. The simulation analysis was carried out using Microsoft Excel 2002 and fitting the curves obtained assuming the rate laws and rate constants. The stopped-flow experiments were carried out at room temperature (ca. 25 °C). For each reaction, good reproducibility of the decay curves was confirmed by performing over five runs, and the determined rate constants were identical to two significant figures. Thus, the rate constant value of each reaction was described to two significant figures.

For the product analysis, we observed the mass spectra using a liquid chromatography−mass spectroscopy (LC−MS) apparatus, Bruker Esquire 3000 Plus (Germany). The sample solutions were prepared by mixing the AN solutions of PA (or MPA) and $TBPA^{\bullet+}$, which was left for a few days before the LC−MS measurements.

All the measurements were carried out in dehydrated acetonitrile (Wako Chemicals, H_2O < 50 ppm). AN solutions of $TBPA^{\bullet+}$ were prepared as reported previously.[7] As for the substrates, *N*-methyl-*p*-anisidine (Aldrich, 99%), *p*-anisidine (Aldrich 99%), *N*-benzyl-*p*-anisidine (Tokyo Kasei, EP grade), and variamine blue (Tokyo Kasei, GR grade) were used as received.

Results and Discussion

Cyclic Voltammograms of PA and MPA. Figure 1 shows the cyclic voltammograms of PA, MPA, and TBPA. While the voltammogram of TBPA was reversible, those of PA and MPA were irreversible at the scan rate of 100 mV s^{-1} as shown in this figure. This implies that the follow-up chemical reactions of $PA^{\bullet+}$ and $MPA^{\bullet+}$ are fast. As in our previous paper,[8] the cyclic voltammogram of DMPA in AN was almost reversible at the scan rate of 100 mV s^{-1}. Thus, $DMPA^{\bullet+}$, which has two methyl groups on the N atom, is much more inert than $PA^{\bullet+}$ and $MPA^{\bullet+}$ in AN. Such a high inertness of $DMPA^{\bullet+}$ was reported also in the oxidation in aqueous media.[9]

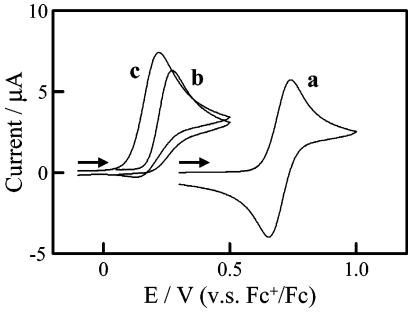

Figure 1. Cyclic voltammograms of (a) TBPA, (b) PA, and (c) MPA in AN. Concentration of substrates, 1.0 mM. Supporting electrolyte, 0.10 M tetrabutylammonium hexafluorophosphate. Working electrode, platinum disk electrode (diameter, 1.6 mm). Scan rate, 100 mV s^{-1}.

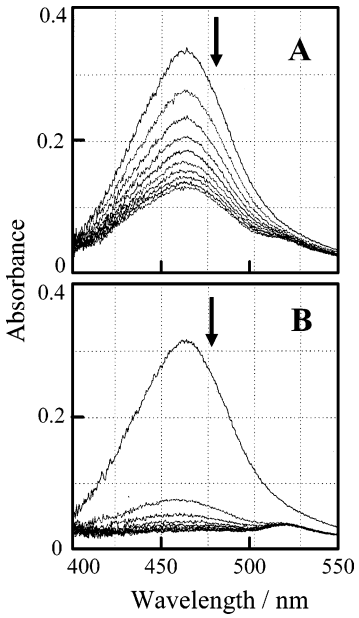

Figure 2. Changes in absorption spectra observed after mixing AN solutions of 0.10 mM $TBPA^{\bullet+}$ with AN solution of MPA. [MPA]: (A) 0.10 and (B) 1.0 mM. Time interval of each spectrum, 0.5 s.

From these voltammograms, we can expect that the electron-transfer reactions of eqs 1 and 2 proceed quantitatively when the solutions are mixed, judging from the sufficient potential difference of ca. 500 mV.

$$PA + TBPA^{\bullet+} \rightarrow PA^{\bullet+} + TBPA \quad (1)$$

$$MPA + TBPA^{\bullet+} \rightarrow MPA^{\bullet+} + TBPA \quad (2)$$

ETSF Observation and Kinetic Results for the Reactions of $MPA^{\bullet+}$. On the basis of eq 2, we mixed an AN solution of 0.10 mM MPA with an AN solution of 0.10 mM $TBPA^{\bullet+}$. As a result, a monotonic decay of visible absorption whose maximum was 460 nm was observed as shown in Figure 2A. Considering the possible quantitative electron transfer of eq 2 and total disappearance of the absorption of $TBPA^{\bullet+}$ just after the mixing, the transformation of absorption spectra can be attributed to the follow-up chemical reaction of $MPA^{\bullet+}$ in solution. In this case, 0.05 mM $MPA^{\bullet+}$ is formed just after the mixing due to equivolume mixing and quantitative electron transfer. The molar absorptivity of $MPA^{\bullet+}$ at 460 nm was determined to be 8.0×10^3 M^{-1} cm^{-1} from the initial absorbance value just after the mixing.

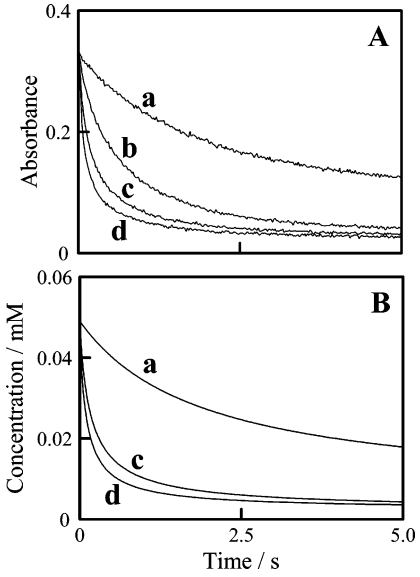

Figure 3. (A) Time changes in absorbance at 460 nm of $MPA^{\bullet+}$ observed after mixing of AN solution of 0.10 mM $TBPA^{\bullet+}$ with AN solution of (a) 0.10, (b) 0.20, (c) 0.50, and (d) 1.0 mM MPA. After mixing, the concentration of MPA coexisting with 0.05 mM $MPA^{\bullet+}$ is (a) 0, (b) 0.05, (c) 0.20, and (d) 0.45 mM, respectively. (B) Simulated results obtained assuming the rate law of (a) $-d[MPA^{\bullet+}]/dt = k[MPA^{\bullet+}]^2$ and (c, d) $-d[MPA^{\bullet+}]/dt = k[MPA^{\bullet+}]^2[MPA]$.

On the other hand, when an AN solution of 1.0 mM MPA was mixed with an AN solution of 0.10 mM $TBPA^{\bullet+}$, accelerated decay of $MPA^{\bullet+}$ was observed as shown in Figure 2B. In this case, the reaction of 0.05 mM $MPA^{\bullet+}$ was initiated in the presence of 0.45 mM MPA after the mixing. Hence, from the difference between Figure 2A and 2B, it was proved that the neutral MPA accelerated the decay reaction of $MPA^{\bullet+}$ significantly.

Compared with our previous results for $DMPA^{\bullet+}$ [8] and *N*,*N*-dimethyl-*p*-toluidine cation radical,[7] it is characteristic in the present results that $MPA^{\bullet+}$ decreased even when only $MPA^{\bullet+}$ was generated without MPA (Figure 2A). In previous work,[8] $DMPA^{\bullet+}$ was quite stable in the absence of DMPA, and, in the presence of DMPA, the rate law of the decay reaction of $DMPA^{\bullet+}$ was determined to be eq 3

$$-d[DMPA^{\bullet+}]/dt = k[DMPA^{\bullet+}][DMPA] \qquad (3)$$

with the second-order reaction rate, *k*, of 8.05 M^{-1} s^{-1}. This rate law was also true for the reaction of the *N*,*N*-dimethyl-*p*-toluidine cation radical.[7]

For the determination of the rate laws involving the present $MPA^{\bullet+}$, we performed simulation analysis for the changes in absorbance at 460 nm, which is the absorption maximum of $MPA^{\bullet+}$, recorded as in Figure 3A. For the decay curve (a) observed when only $MPA^{\bullet+}$ was generated without MPA, a good fit was obtained assuming the second-order decrease of $MPA^{\bullet+}$ (Figure 3B(a)); i.e., the rate law was determined to be eq 4 and the second-order rate constant, *k*, was determined to be 1.2 $\times$ 10^4 M^{-1} s^{-1}.

$$-d[MPA^{\bullet+}]/dt = k[MPA^{\bullet+}]^2 \qquad (4)$$

On the other hand, the acceleration observed in the presence of MPA was confirmed to be due to the mechanistic change. For decay curves c and d observed with some excesses of MPA in Figure 3A, well-fitted results could be obtained assuming the rate law of eq 5, and the third-order rate constants of 6.1 $\times$ 10^8 and 4.2 $\times$ 10^8 M^{-2} s^{-1} for curves c and d, respectively.

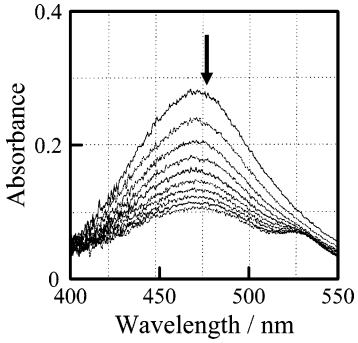

Figure 4. Changes in absorption spectra observed after mixing AN solution of 0.10 mM $TBPA^{\bullet+}$ with AN solution of 0.10 mM BPA. Time interval of each spectrum, 0.8 s.

$$-d[MPA^{\bullet+}]/dt = k[MPA^{\bullet+}]^2[MPA] \qquad (5)$$

At the intermediate condition, i.e., [MPA] after the mixing was 0.05 mM (Figure 3A(b)), no good curve fit was obtained assuming only eq 4 or 5. This would be due to the reason that both reactions of eqs 4 and 5 contribute to the decay process of $MPA^{\bullet+}$. Actually, assuming the contributions of both rate laws, we could predict the decay curve of Figure 3A(b).

When the concentrations of MPA after the mixing were 0.95 and 2.45 mM, the rate constants were determined to be 3.8 $\times$ 10^8 and 2.9 $\times$ 10^8 M^{-2} s^{-1}, respectively. From the rate constant values decreasing with the increase of [MPA], it is expected that there are some contributions of eq 4 to the determination of the *k* values of eq 5, even when [MPA] after the mixing is over 0.20 mM.

ETSF Observation and Kinetic Results for the Reactions of $BPA^{\bullet+}$. In the same manner, we observed the decay reactions of $BPA^{\bullet+}$ in AN. Figure 4 shows the changes in absorption spectra observed after mixing AN solutions of 0.10 mM BPA and 0.10 mM $TBPA^{\bullet+}$. As shown in this figure, we could observe a monotonic decay that is very similar to that of $MPA^{\bullet+}$ (Figure 2A), but a slight deceleration of the decay reaction was recognized from the time interval of 0.8 s in Figure 4. The simulated result for the decay curve of $BPA^{\bullet+}$ without BPA showed that the rate law is identical to eq 4, and the rate constant, *k*, was 5.3 $\times$ 10^3 M^{-1} s^{-1}. This value is 43% that of $MPA^{\bullet+}$.

Also, the rate law obtained for the decay curve of $BPA^{\bullet+}$ with the presence of 0.45 mM BPA was identical to eq 5, and the rate constant was 1.1_5 $\times$ 10^8 M^{-2} s^{-1}, which is 28% that of $MPA^{\bullet+}$.

ETSF Observation and Kinetic Results for the Reactions of $PA^{\bullet+}$. While the monotonic decay profiles were observed for $MPA^{\bullet+}$ and $BPA^{\bullet+}$ in the visible region as shown in Figures 2 and 4, different transformations of visible absorption spectra were recorded for the cases of $PA^{\bullet+}$. When 0.05 mM $PA^{\bullet+}$ was generated without PA, the decrease of an absorption at 450 nm, which can be attributed to the absorption peak of $PA^{\bullet+}$, was observed accompanying the increase of broad absorption around 580 nm. On the other hand, when 0.05 mM $PA^{\bullet+}$ was generated in the presence of 0.45 mM PA, a significant acceleration of the decay process of $PA^{\bullet+}$ was observed as in Figure 5B. In addition, the suppressed increase of the absorption around 580 nm was confirmed compared with the transformation in Figure 5A.

Figure 6 shows the time changes in absorbance values at 450 and 580 nm for the result of Figure 5A. In the reaction of the

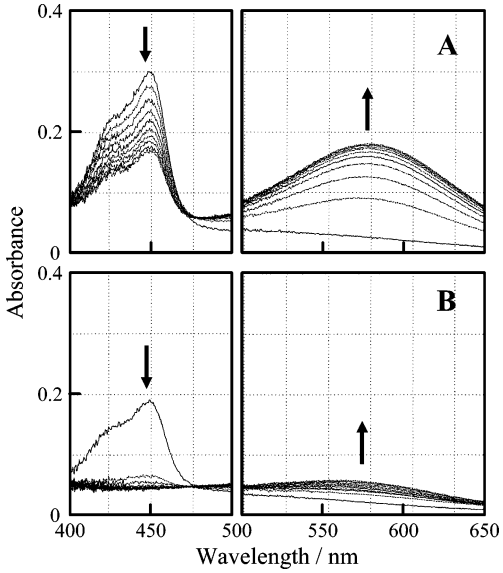

Figure 5. Changes in absorption spectra observed after mixing AN solution of 0.10 mM $TBPA^{\bullet+}$ with AN solution of PA. [PA]: (A) 0.10 and (B) 1.0 mM. Time interval of each spectrum, 0.05 s.

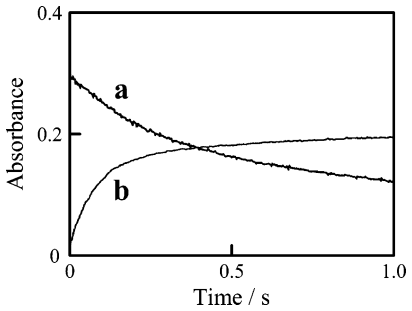

Figure 6. Time changes in absorbance at (a) 450 and (b) 580 nm for 1.0 s after mixing AN solution of 0.10 mM $TBPA^{\bullet+}$ with AN solution of 0.10 mM PA. The wavelengths correspond to the absorption maxima of (a) $PA^{\bullet+}$ and (b) VB^{2+}, respectively.

methyldiphenylamine cation radical in AN,[5] symmetrical decrease and increase of the monomer cation radical (reactant) and the dimer cation radical (product) were observed concurrently, which implied fast electron-transfer reaction after the dimer formation, which was the rate-determining step. In contrast, in the present case, the increase of the absorption at 580 nm seems to be steeper than the decrease of $PA^{\bullet+}$, which cannot be explained assuming simple conversion of $PA^{\bullet+}$ into the product. Thus, the complexity of the reaction process is expected for the reactions of $PA^{\bullet+}$, in particular, after the rate-determining step.

However, for the decreasing process of $PA^{\bullet+}$ (Figure 6a), the result of simulation analysis showed an excellent fit, and consequently, the rate law was determined to be

$$-\mathrm{d}[PA^{\bullet+}]/\mathrm{d}t = k[PA^{\bullet+}]^2 \qquad (6)$$

with the rate constant, k, of $4.10 \times 10^4\ M^{-1}\ s^{-1}$. Thus, the decay kinetics of $PA^{\bullet+}$ was the same as that of $MPA^{\bullet+}$ in the absence of the neutral molecules, though the increase of the absorption of the product was observed only for $PA^{\bullet+}$, not for $MPA^{\bullet+}$.

Figure 7 shows the decay curves of $PA^{\bullet+}$ at 450 nm recorded in the presence of PA. The acceleration of the decay reactions of $PA^{\bullet+}$ by the neutral PA was recognized compared with Figure 6. Although the slight increases of absorbance with time can be seen for curves b and c, which would be due to the increase of the broad absorbance around 580 nm, the successful

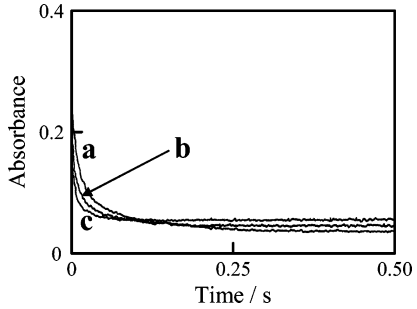

Figure 7. Time changes in absorbance at 450 nm of $PA^{\bullet+}$ observed after mixing AN solution of 0.10 mM $TBPA^{\bullet+}$ with AN solution of (a) 0.50, (b) 1.0, and (c) 2.0 mM PA. After mixing, the concentration of PA coexisting with 0.05 mM $PA^{\bullet+}$ is (a) 0.20, (b) 0.45, and (c) 0.95 mM, respectively.

simulation analysis could be performed for the initial decay processes of $PA^{\bullet+}$. As a consequence, the rate law was determined to be eq 7, and the rate constants were 1.35×10^{10} and $1.10 \times 10^{10}\ M^{-2}\ s^{-1}$ for the presence of 0.20 and 0.45 mM PA, respectively.

$$-\mathrm{d}[PA^{\bullet+}]/\mathrm{d}t = k[PA^{\bullet+}]^2[PA] \qquad (7)$$

In the presence of PA, the obtained rate law was also identical to that of $MPA^{\bullet+}$. However, the reaction of $PA^{\bullet+}$ involving PA was much faster than that of $PA^{\bullet+}$ without PA, which is in contrast to the results of $MPA^{\bullet+}$. Additionally, it was characteristic that the absorption due to the reaction product became smaller compared with the result for the reaction of $PA^{\bullet+}$ without PA.

Cyclic Voltammetric Observation for the Reaction Products. To obtain information concerning the product in the reactions of $PA^{\bullet+}$, we observed a cyclic voltammogram of variamine blue (VB).

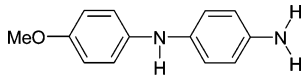

VB

Figure 8 shows the CV of VB in AN together with the voltammogram of PA, for which the scan was repeated. As studied in detail by Bewick et al.,[10] a two one-electron oxidation of VB was confirmed in AN. The small redox couple appearing in Figure 8A(b) would be attributed to that of the $VB/VB^{\bullet+}$ couple. Thus, it is inferred that VB is formed in the electrochemical oxidation of PA in AN.

While the data are not shown here, in the cyclic voltammograms of MPA, no redox waves of the product similar to that of PA was observed in the repeated scans. Because the 1,4-diamine structure usually permits formation of stable cation radicals in AN, it is inferred that a structure similar to VB is not formed in the reaction of $MPA^{\bullet+}$, while the kinetic results are similar in both cases.

Absorption Spectra of Oxidation States of VB. Although the absorption spectra of $VB^{\bullet+}$ and VB^{2+} have been reported previously,[10] these absorption spectra can be easily obtained in the ETSF method as well through the mixing with $TBPA^{\bullet+}$. That is, when AN solutions of 0.10 mM $TBPA^{\bullet+}$ and 0.10 mM VB are mixed, 0.05 mM $VB^{\bullet+}$ is formed; similarly, 0.025 mM VB^{2+} can be formed by mixing AN solutions of 0.10 mM $TBPA^{\bullet+}$ and 0.05 mM VB. These are supported by the oxidation potentials of TBPA, VB, and $VB^{\bullet+}$ and the stability of $VB^{\bullet+}$ and VB^{2+} in Figure 8. Actually, in this manner, we could

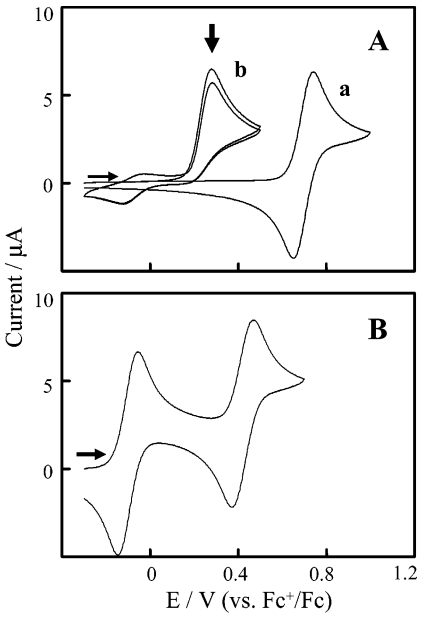

Figure 8. Cyclic voltammograms of (A) (a) TBPA and (b) PA, and (B) VB in AN. Concentration of substrates, 1.0 mM. Supporting electrolyte, 0.10 M tetrabutylammonium hexafluorophosphate. Working electrode, platinum disk electrode (diameter, 1.6 mm). Scan rate, 100 mV s^{-1}.

observe the absorption spectra of $VB^{\bullet+}$ and VB^{2+}. The absorption maximum of $VB^{\bullet+}$ was 580 nm ($\epsilon = 2.1 \times 10^4$ M^{-1} cm^{-1}) and that of $VB^{\bullet+}$ was 595 nm ($\epsilon = 7.5 \times 10^3$ M^{-1} cm^{-1}). While the broad absorptions of both species resemble each other, the absorption in Figure 5A was quite similar to that of VB^{2+}.

Supposing the formation of only VB^{2+}, not $VB^{\bullet+}$, the calculated result for the absorbance at 580 nm in Figure 5A showed that 0.010 mM VB^{2+} was formed with the decrease of 0.024 mM $PA^{\bullet+}$. If VB^{2+} is quantitatively formed via eq 8

$$PA^{\bullet+} + PA^{\bullet+} \rightarrow VB^{2+} + MeOH \qquad (8)$$

the formation of VB^{2+} is a little smaller than the expected value. Moreover, the smaller absorption in Figure 5B is difficult to evaluate only assuming the formation of $VB^{\bullet+}$ or VB^{2+}. Supposing the simplest overall reaction of eq 9, the absorbance value of 0.155 should be obtained for the generation of $VB^{\bullet+}$ at 595 nm.

$$PA^{\bullet+} + PA \rightarrow VB^{\bullet+} + MeOH \qquad (9)$$

Concluding Discussion for the Reaction Mechanisms. In the present work using the ETSF method, systematic kinetic results could be obtained for the initial decay processes of *p*-anisidine derivative cation radicals, including $PA^{\bullet+}$, $MPA^{\bullet+}$, $BPA^{\bullet+}$, and the previous $DMPA^{\bullet+}$.[8] By the substitution of the methyl group(s) on the N atom into −H, the reactions of the cation radicals were accelerated significantly accompanying the changes in the rate law, i.e., the changes in the reaction mechanisms.

Among these derivatives, the reaction of $DMPA^{\bullet+}$ might be an exceptional case, because the dimerization proceeds via the C−C bonding between two *N*-methyl groups.[8] Kinetically, the rate law was eq 3, which indicates the acid−base interaction between $DMPA^{\bullet+}$ and DMPA.

Comparing with the slow reaction rate of $DMPA^{\bullet+}$ with DMPA,[8] the faster reactions of $MPA^{\bullet+}$ indicate that the reactions do not proceed via the C−C bonding. Actually, in the product analysis using LC−MS, it was found that the main product of the reaction of $MPA^{\bullet+}$ was the cyclized dimer formed via the N−C bonding (N−C dimer). Although the formation of the

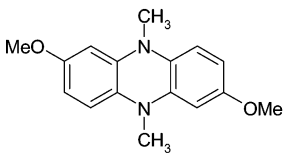

N-C dimer

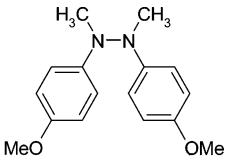

N-N dimer

N−N bonded dimer might be possible as in previous work on the chemical oxidation of MPA with $Tl(OAc)_3$ in nitromethane,[11] the mass results showed that four protons was eliminated in the product dimer.

The kinetic results for $BPA^{\bullet+}$, which were very similar to those for $MPA^{\bullet+}$, would be a support for the reaction route to form the cyclized dimer. If we suppose other reaction routes, a large structural hindrance of $BPA^{\bullet+}$ might decelerate the reaction. In addition, no formation of the trimer or oligomer was found in the mass results, which indicate that further reactions of the dimer do not proceed in the case of $MPA^{\bullet+}$.

Kinetically, the acceleration of the reaction of $MPA^{\bullet+}$ with MPA can be expected on the basis of Scheme 1.

SCHEME 1

$$MPA + MPA^{\bullet+} \rightleftharpoons (MPA)_2^{\bullet+} \qquad (10)$$

$$(MPA)_2^{\bullet+} + MPA^{\bullet+} \rightarrow (MPA)_2^{2+} + MPA \qquad (11)$$

$$(MPA)_2^{2+} \rightarrow \rightarrow \text{N-C dimer} + 4H^+ \qquad (12)$$

Scheme 2 would be also possible to form the same intermediate, which is a probable explanation for the second-order rate

SCHEME 2

$$2MPA^{\bullet+} \rightarrow (MPA)_2^{2+} \rightarrow \rightarrow \text{N-C dimer} + 4H^+ \qquad (13)$$

law of eq 4 for the reaction of $MPA^{\bullet+}$ without MPA. In Figure 9, the reaction mechanisms of these schemes are summarized with structures, though the proton-releasing steps might be in the stages prior to the formation of $(MPA)_2^{2+}$.

The concurrent occurrence of both schemes is possible when the amount of the coexisting MPA is relatively small. Thus, the slight decrease of the rate constants with the increase of [MPA] is inferred to be observed, though the mechanistic change could be confirmed between eq 4 and eq 5.

For the reactions of $PA^{\bullet+}$, whole reaction processes would be more complicated judging from the absorption of the product recorded in the ETSF observation (Figure 5). While the product was assumed as VB^{2+} in a previous report using fast-scan cyclic voltammetry,[3] the almost quantitative conversion to VB^{2+} was observed only when $PA^{\bullet+}$ was generated without PA in the conditions of the ETSF measurements. In addition, while the rate law was found to be first order in both [$PA^{\bullet+}$] and [PA] in DMF as the significant effect of the neutral molecule,[3] our results in AN have given the different rate laws of eqs 6 and 7 despite the similarity that PA accelerated the decay reaction of $PA^{\bullet+}$ significantly.

Here, it should be stressed that there is a huge difference between the electrochemical oxidation reactions and the reactions in homogeneous solution in the ETSF method. In electrode oxidation, positive charges are supplied to species in the vicinity of the surface from the electrode depending on the electrode

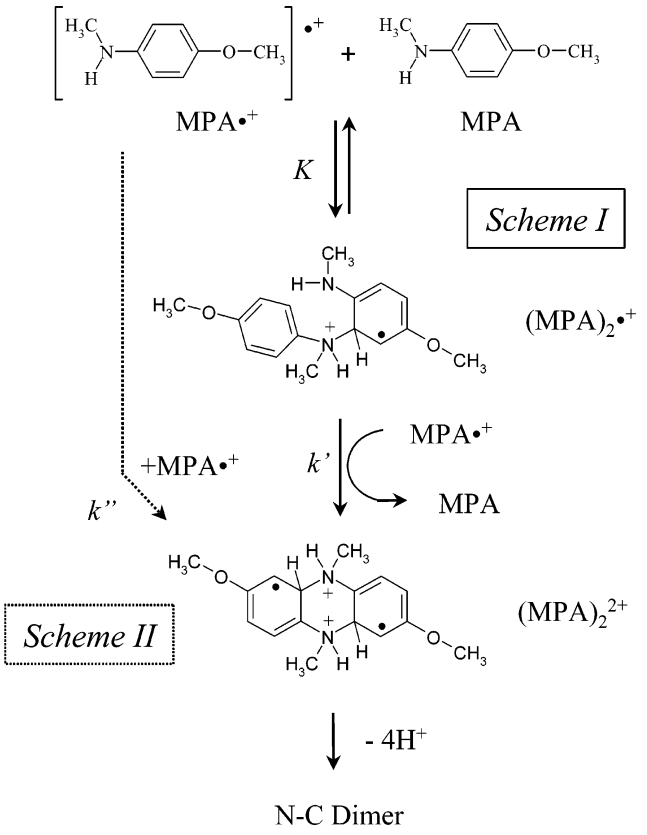

Figure 9. Reaction mechanisms of $MPA^{\bullet+}$ to form N−C dimer. Based on the kinetic results, both routes are possible to form $(MPA)_2^{2+}$. The reaction rates, k, in eqs 4 and 5 can be expressed as $2k''$ and $2Kk'$, respectively, using the values in this figure.

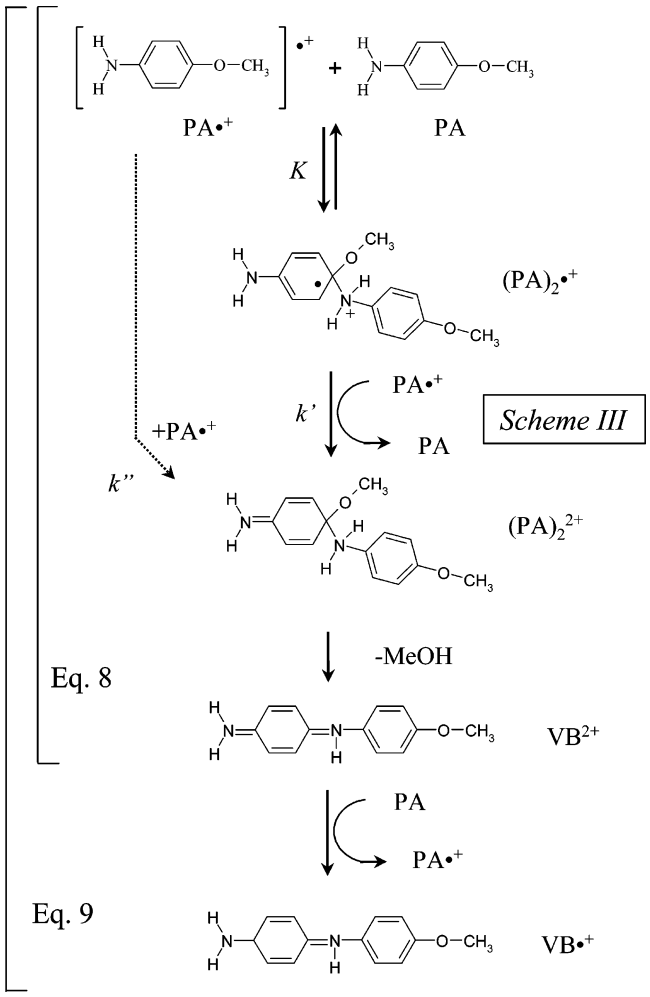

Figure 10. Reaction mechanisms of $PA^{\bullet+}$ to form VB^{2+} and $VB^{\bullet+}$. The overall stoichiometries to form VB^{2+} and $VB^{\bullet+}$ are expressed by eqs 8 and 9, respectively. Based on the kinetic results, a simple interaction betwee $PA^{\bullet+}$ and PA to form $VB^{\bullet+}$ can be ruled out despite the overall stoichiometry of eq 9. The reaction rates, k, in eqs 6 and 7 can be expressed as $2k''$ and $2Kk'$, respectively, using the values in this figure.

potential; however, in the ETSF measurement, the positive charge supplied into the solution is constant and is restricted to be a very small amount even in the presence of a large excess of neutral molecules. Additionally, the solvents used are different, and the supporting electrolytes are present in the electrochemical oxidation. Thus, here, as the mechanistic conclusions for the reactions of $PA^{\bullet+}$ in homogeneous AN solutions, we would like to propose the rate laws of eqs 6 and 7.

Kinetically, the second-order reaction for $[PA^{\bullet+}]$ in the rate law of eq 6 can be essentially assigned to the reaction between two $PA^{\bullet+}$ ions to form VB^{2+} (eq 8). On the other hand, for the rate law of eq 7, Scheme 3 would be a reasonably expected

SCHEME 3

$$PA + PA^{\bullet+} \rightleftharpoons (PA)_2^{\bullet+} \quad (14)$$

$$(PA)_2^{\bullet+} + PA^{\bullet+} \rightarrow (PA)_2^{2+} + PA \quad (15)$$

$$(PA)_2^{2+} \rightarrow VB^{2+} + MeOH \quad (16)$$

$$VB^{2+} + PA \rightarrow VB^{\bullet+} + PA^{\bullet+} \quad (17)$$

mechanism because the simple and direct interaction between PA and $PA^{\bullet+}$ to form $VB^{\bullet+}$ would not give the results of second-order dependence for $[PA^{\bullet+}]$.

In Figure 10, the possible reaction mechanisms are summarized with structures. Here, after forming VB^{2+}, the reduction of VB^{2+} by PA is expected to form $VB^{\bullet+}$ and $PA^{\bullet+}$ (eq 17), which is reasonable based on the formal potentials of the redox couples of $VB^{\bullet+}/VB^{2+}$ and $PA/PA^{\bullet+}$ (Figure 8). While the overall stoichiometry to form $VB^{\bullet+}$ is expressed by eq 9, a simple mechanism in which $PA^{\bullet+}$ interacts with PA to form $VB^{\bullet+}$ can be ruled out based on the kinetic results.

Although we discussed the mechanisms only on the basis of the decreasing kinetics of $PA^{\bullet+}$ at the initial stage, the results of the product analysis showed that the overall reaction was not simple. Actually, VB^{2+} or $VB^{\bullet+}$ could be detected in the absorption spectra of Figure 5, and the electrochemical result of Figure 8 supported the formation of $VB^{\bullet+}$. However, in the result of LC−MS measurement, VB was not detected but the products with higher mass number were detected in the reactant solution, implying the follow-up reactions of $VB^{\bullet+}$. Thus, after the rate-determining step of the decay reactions of $PA^{\bullet+}$, some slow reactions are expected to occur.

As mentioned in the previous section, the absorbance values of VB^{2+} and $VB^{\bullet+}$ in Figure 5B were smaller than the values expected assuming their quantitative formation. The presence of the follow-up reactions might be one of the reasons for the smaller values. As another reason, the deprotonation from VB^{2+} and $VB^{\bullet+}$ by the neutral molecule would be inferred as reported in a previous paper.[10]

Conclusions

Kinetic analysis for the reactions of $PA^{\bullet+}$, $MPA^{\bullet+}$, and $BPA^{\bullet+}$ was carried out, and the results were systematically compared including previous results obtained for the reactions of $DMPA^{\bullet+}$.[8] For the *p*-anisidine derivative cation radicals, in which the reactive para position is blocked by the methoxy group, it was found that two *N*-methyl groups on the N atom decelerate the dimerization significantly. In this case of $DMPA^{\bullet+}$, the C−C bonding of the *N*-methyl groups was the sole reaction route, and the reaction was promoted by the acid−base interaction between $DMPA^{\bullet+}$ and DMPA.

The substitution of the methyl group on the N atom into −H brought about significant increases in the reactivity of the cation radicals. In addition, for both $PA^{\bullet+}$ and $MPA^{\bullet+}$, the acceleration of the decay reactions of the cation radical by the presence of neutral molecules was clearly observed. ETSF observation permitted the determination of the rate laws and the rate constants for all reactions in homogeneous AN solutions, though the reaction processes after the rate-determining step seemed to be complicated.

The comparisons of the reactivity of the aniline derivative cation radicals such as those in the present work would be useful for considering the formation processes of conducting polymers. In addition, some mechanistic differences between the heterogeneous electrochemical reactions and the homogeneous reactions in solution were demonstrated in the present work using the ETSF method.

Acknowledgment. This work was supported in part by a Grant-in-Aid for Scientific Research from the Ministry of Education, Culture, Science, Sports and Technology, Japan, No. 13640602. X.C. and M.O. thank the Kyoto University Foundation for the support of the research visit of X.C. to Kyoto University.

References and Notes

(1) Yang, H.; Bard, A. J. *J. Electroanal. Chem.* **1991**, *306*, 87.
(2) Andrieux, C. P.; Gallardo, I.; Junca, M. *J. Electroanal. Chem.* **1993**, *306*, 231.
(3) Simon, P.; Farsang, G.; Amatore, C. *J. Electroanal. Chem.* **1997**, *435*, 165.
(4) Amatore, C.; Farsang, G.; Maisonhaute, E.; Simon, P. *J. Electroanal. Chem.* **1999**, *462*, 55.
(5) Oyama, M.; Higuchi, T.; Okazaki, S. *J. Chem. Soc., Perkin Trans. 2* **2001**, 1287.
(6) Oyama, M.; Matsui, J.; Park, H. *Chem. Commun*. **2002**, 604.
(7) Goto, M.; Park, H.; Otsuka, K.; Oyama, M. *J. Phys. Chem. A* **2002**, *106*, 8103.
(8) Oyama, M.; Goto, M. *Indian J. Chem. A* **2003**, *42*, 8103.
(9) Bacon, J.; Adams, R. N. *J. Am. Chem. Soc.* **1968**, *90*, 6596.
(10) Bewick, A.; Serve, D.; Joslin, T. A. *J. Electroanal. Chem.* **1983**, *154*, 814.
(11) Cimainale, F. *Tetrahedron Lett.* **1994**, *35*, 3375.